

ADVANCED MATERIALS

Supporting Information

for *Adv. Mater.*, DOI 10.1002/adma.202414617

Symmetry is the Key to the Design of Reticular Frameworks

*Andrea Darù**, John S. Anderson, Davide M. Proserpio and Laura Gagliardi*

Supporting Information:

Symmetry is the key to the design of reticular frameworks

Andrea Darù,^{*,†} John S. Anderson,[†] Davide M. Proserpio,[‡] and Laura Gagliardi^{*,†,¶}

[†]*Department of Chemistry, University of Chicago, Chicago, Illinois 60637, United States*

[‡]*Dipartimento di Chimica, Università degli studi di Milano, Via Golgi 19, 20133 Milano, Italy*

[¶]*Pritzker School of Molecular Engineering, University of Chicago, Chicago, Illinois 60637, United States*

E-mail: adaru@uchicago.edu; lgagliardi@uchicago.edu

Contents

1	Computational Details	S2
1.1	MOF and COF periodic calculations	S2
1.2	Molecular calculations of nodes and linkers	S2
2	ARC-derived and experimental datasets	S3
3	Workflow Details	S4
3.1	MOF-801, MOF-802, MOF-841, MOF-808	S4
3.2	MOF-812	S6

3.3	NU-50	S7
3.4	PCN-6'	S8
3.5	LZU-306	S10
3.6	LZU-111	S12
4	CSD Refcodes	S12

1 Computational Details

1.1 MOF and COF periodic calculations

The Vienna Ab initio Simulation Package (VASP) version 6.4.0¹⁻³ was used for all the plane-wave density functional theory (DFT) calculations performed in this study using the functionals Perdew-Burke-Ernzerhof PBE exchange-correlation density functional⁴ along with Grimme’s D3 dispersion correction with Becke-Johnson damping (D3BJ),⁵ and r²SCAN⁶ with non-local correlation functional rVV 10 that approximately accounts for dispersion interactions⁷ to optimize the atomic positions and lattice parameters of MOF and COF respectively. In every case, the standard PAW pseudopotentials⁸ were used for all atoms present in the MOF and COF structures optimized. A 520 eV energy cutoff, a 10⁻⁶ eV self-consistent field (SCF) threshold, a 0.01 eV/Å forces threshold, and 0.01 eV Gaussian smearing were used. A 1 x 1 x 1 k-mesh was used for all MOF geometry optimization beside NU-50 where 2 x 2 x 1 and 3 x 3 x 1 were used for **pts**-NU-50 and **pth**-NU-50 respectively. A 2 x 2 x 1 k-mesh was used for all COF structures LZU-111 in every topology.

1.2 Molecular calculations of nodes and linkers

Molecular calculations were performed in gas phase using Kohn Sham density functional theory (KS-DFT) with Gaussian 16 rev. B.01.⁹ Geometry optimization was performed employing the hybrid functional TPSSh^{10,11} including the empirical dispersion correction with

Becke and Johnson damping function D3BJ.⁵ The Ahlrichs basis set def2-SVP¹² was used for geometry optimization for all atoms. The keyword "symmetry=on" was used in all calculations to request a symmetry oriented geometry optimization.

2 ARC-derived and experimental datasets

The frequency of occurrence ranking dataset is made from pieces of information extracted from the structures (cif files) present in the ARC database¹³ which are used to build a different dataset that records the repetition of each topology, extracted by us using the single node method¹⁴ from each cif file. Also, an only experimental dataset is also made by using structures from CoRE MOF¹⁵ and CSD^{16,17} databases avoiding duplicates. The underlying topology as single-node of each structure is then extracted, after symmetrization, and compiled into the two new datasets containing only the topology name and its frequency of occurrence which we refer as ARC-derived dataset and experimental dataset.

The original ARC database contains 521381 MOF structures as cif files, from which 466223 are remain after removing 55158 of them from which it was impossible to extract their topology. These 466223 structures were used to make the ARC-derived dataset which contains the frequency of occurrence of the underlying topology of such structures. The ARC-derived dataset contains 829 different topologies, the most frequent of them are shown in the main text. Similarly, the experimental dataset has been created by topology extraction from 7334 experimental structures: 4844 from CoRE MOF and 2490 from CSD database following the selection from ARC database. In this dataset there are 258 different topologies.

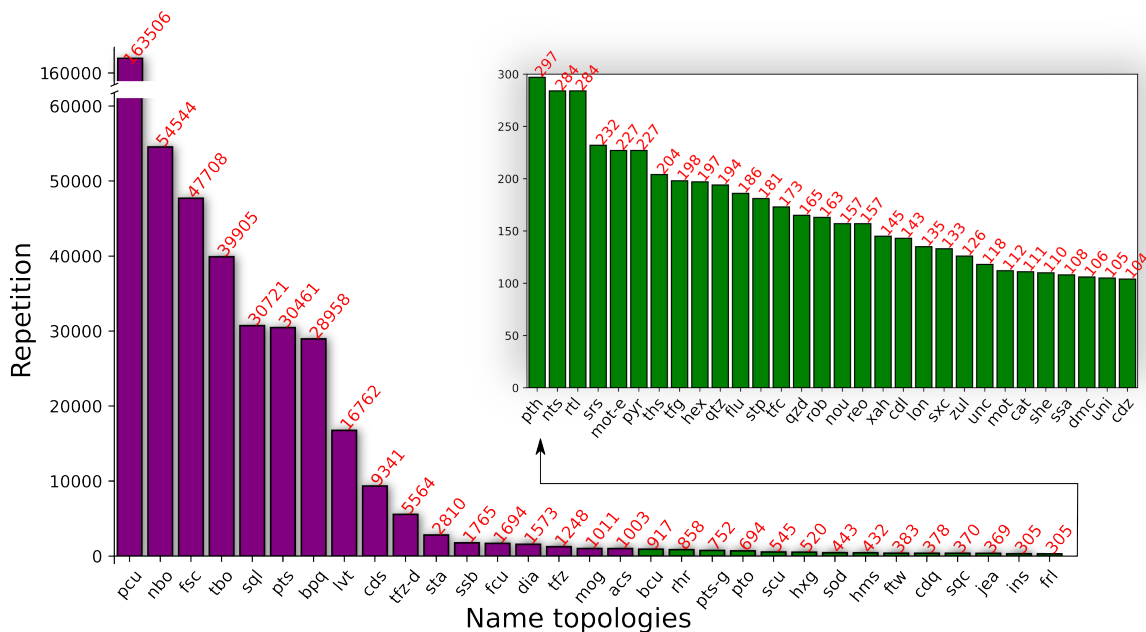


Figure S1: Ranking of topologies from ARC-derived dataset. The two plots show the 61 most frequent topologies divided into two plots with repetition of at least 100 times. The 17 most frequent topologies are highlighted in purple with repetition of at least 1000 times.

3 Workflow Details

3.1 MOF-801, MOF-802, MOF-841, MOF-808

The node SBUs of MOF-801, MOF-802, MOF-841, MOF-808 have been generated by the geometry optimization of the MOF-801 node, which is formed by 12 formate moieties surrounding the $\text{Zr}_6\text{O}_4(\text{OH})_4$ core (Figure S3 top). After geometry optimization the H atoms belonging to the formate moieties have been substituted with 12 X atoms to provide 12 connections; to create the node of MOF-802 10 H atoms have been substituted with X to provide 10 connections; the same for MOF-841 with 8 connections; and MOF-808 with 6 connections (Figure S3 bottom).¹⁸

MOF-841¹⁸ has been described in the main text therefore here is not repeated, its node is shown in Figure S3 the third structure from the left with 8 connections and symmetry D_{4h} .

MOF-801 is formed by the 12-connections node of Figure S3 and a 2-connections linker,

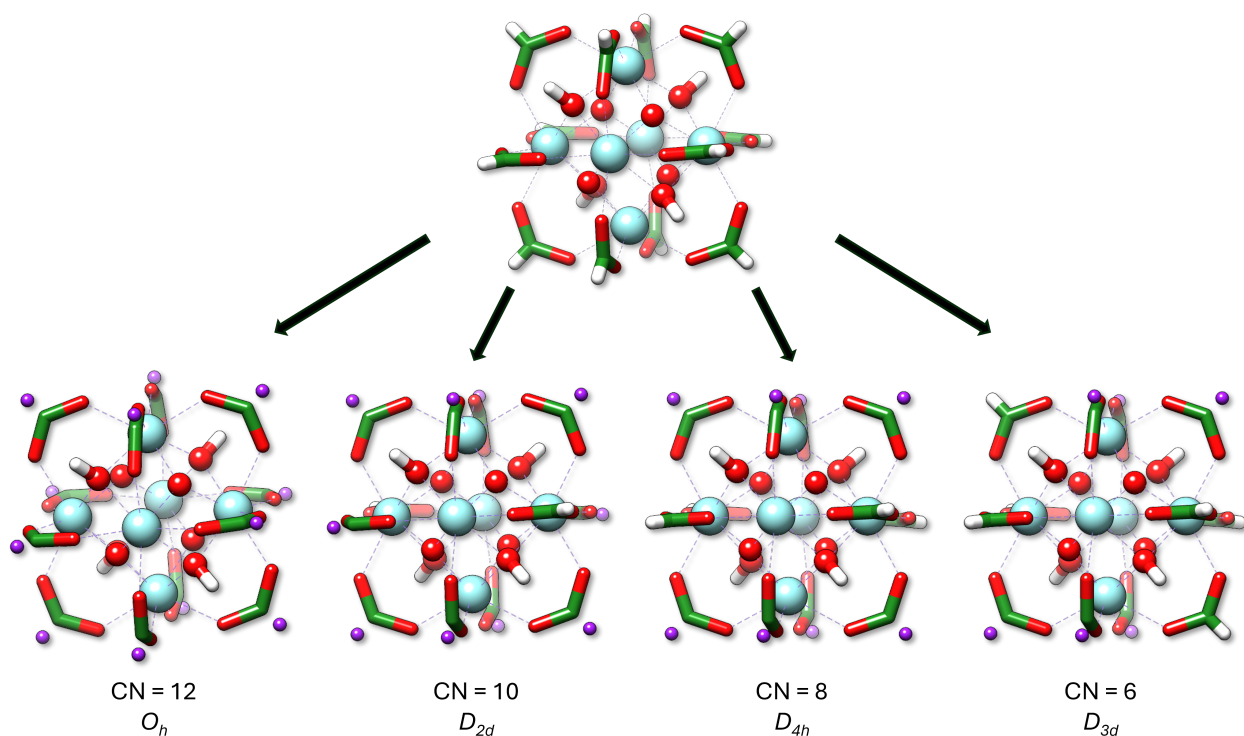


Figure S2: Node of MOF-8XX family optimized structure (top). Node SBUs of, bottom from left to right, MOF-801, MOF-802, MOF-841, MOF-808. Colorcode: Zr cyan, O red, C green, H white, X purple.

similarly to UiO-66,¹⁹ MOF-804, MOF-805, and MOF-806.¹⁸ With a symmetry O_h together with fumaric acid as linker the possible topologies, from connections number only, are **nbo-x**, **ibb**, **ild**, **lcz**, **thp-x**, **fcu**, **xii**, **hcp** from which after applying the symmetry and occurrence modules, **fcu** was the only topology coming out; in agreement with experimentally reported structure.

MOF-802¹⁸ formed by a 10-connections node (second from the left in Figure S3) with symmetry D_{2d} and, as MOF-801, a 2-connections linker has the following available topologies, from connections number only, **lcw-x**, **hxxg-d**, **srr**, **bct** from which after the symmetry and occurrences modules **bct** was the only one coming out; in agreement with experimentally reported structure.

MOF-808¹⁸ is formed by a 6-connections node and symmetry D_{3d} (last from Figure S3), with the trigonal 3-connections linker H₂BTC (1,3,5-benzenetricarboxylate) and symmetry

D_{3h} . The pairing of these two elements provide, from connections number only, the following topologies: **lvs**, **act**, **edq**, **dag**, **spn**, **ttp**, **hwx**, **cdj**, **nha**, **pyr**, **ant**, **rtl**, **ydq**, **svn-d**, **tsx**, **lnj**, **czz**, **ith-d**, **ttx**, **ibe**, **eea**, **anh**, **sit**, **xab** from which, after the symmetry and occurency modules only **spn** is a good fit; in agreement with experimentally reported structure.

3.2 MOF-812

MOF-812¹⁸ belongs to the same family of MOFs described in the previous section, however due to the defects of the coordination of the linker with the node the workflow fails to identify the correct topology. The detected symmetry of this node is C_1 but instead it should be either T_h or T to provide the correct final MOF topology. In this sense, the workflow needs to be improved for defective nodes so to account for every type of reticular frameworks.

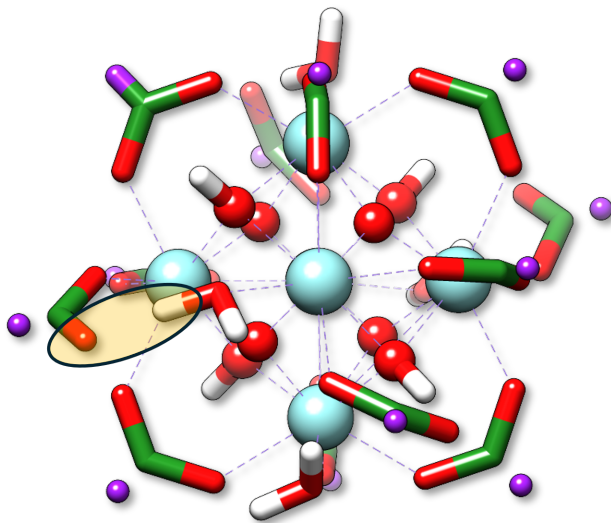


Figure S3: Node of MOF-812 DFT optimized with TPSSh-D3BJ/Def2-SVP. The circle highlights the uncoordinated carboxyl group to the Zr center, that instead hydrogen-bond to the nearby water molecule. Colorcode: Zr cyan, O red, C green, H white, X purple.

3.3 NU-50

As discussed in the main text, **ssb**-NU-50 was found to be about 10.9 kcal/mol higher than **pts**-NU-50 in electronic energy terms. Therefore, from the **ssb** DFT optimized structure the computational PXRD pattern has been calculated and shown in Figure S5 for comparison. The structures chosen for **ssb**-NU-50 and **pts**-NU-50 in this section have been optimized with Na^+ as counterion to save in computational time. The higher peak from the **ssb** PXRD pattern²⁰ shows a shift towards the left from the **pts** one, therefore not matching the experimental shift towards the right as done for **pth**. From this comparison it is clear that the **ssb** topology, because of the energy gap from **pts**, and the PXRD shift, cannot be present in the final product neither after activation.

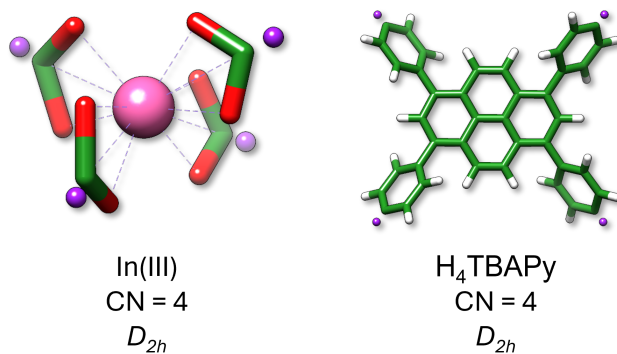


Figure S4: SBUs building blocks of MOF NU-50

The full list of the 241 available topologies for a combination of node and linker with 4 coordinations each is: **afx**, **afy**, **aht**, **apc**, **apd**, **asf**, **ast**, **asv**, **att**, **atv**, **aww**, **baa**, **bab**, **bac**, **baf**, **bag**, **bah**, **baj**, **bak**, **bal**, **bam**, **ban**, **bao**, **bap**, **baq**, **bar**, **bas**, **bat**, **bau**, **bav**, **baw**, **bax**, **bay**, **baz**, **bba**, **bbb**, **bbc**, **bbd**, **bbe**, **bbf**, **bbg**, **bbh**, **bbi**, **bbj**, **bbk**, **bbm**, **bbn**, **bbo**, **bbp**, **bbq**, **bbv**, **bbw**, **bbx**, **bby**, **bbz**, **bca**, **ccb**, **bcd**, **bce**, **bcf**, **bcj**, **bck**, **bcm**, **bcn**, **bco**, **bcp**, **bcq**, **bcv**, **bcw**, **bcx**, **bcy**, **bcz**, **bda**, **bel**, **bik**, **bne**, **bnl**, **bow**, **brl**, **bsv**, **byl**, **cbt**, **cda**, **cdm**, **cdn**, **cdp**, **cdz**, **cfc**, **coe**, **css**, **cua**, **cus**, **eab**, **edi**, **edp**, **eri**, **fel**, **fgl**, **frl**, **ftc**, **ftd**, **fte**, **ftf**, **ftg**, **fth**, **fti**, **ftj**, **ftk**, **ftl**, **ftm**,

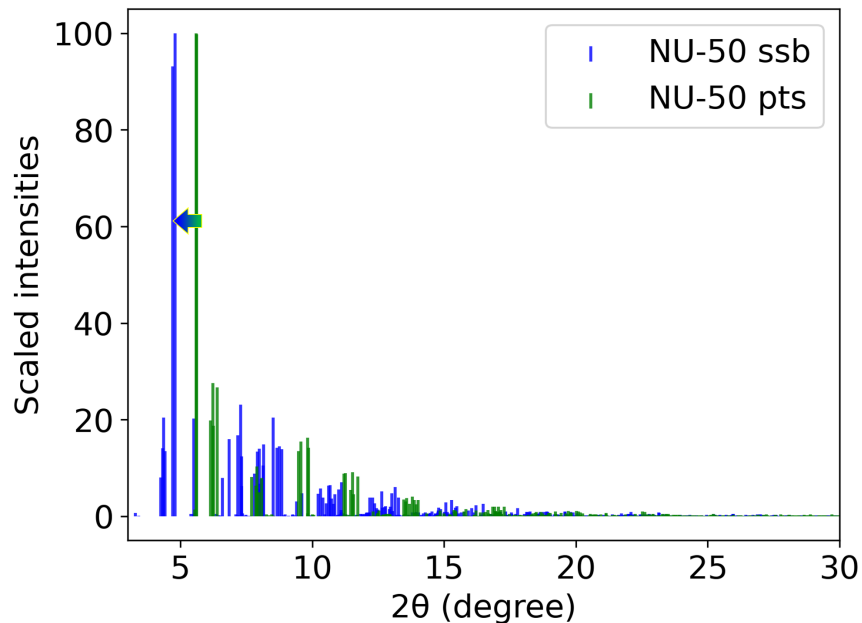


Figure S5: PXRD pattern comparison, from computation, of **ssb**-NU-50 (blue). and **pts**-NU-50 (green).

ftn, fto, ftp, ftq, ftr, fts, ftt, ftu, ftv, ftx, fty, ftz, fua, fub, fud, fue, fuf, fug, fuh, fuj, ful, fum, fun, fuo, fup, fur, fus, fut, fuu, fuv, fuw, fuy, fuz, fva, fvb, fvc, fvd, fve, fvf, fvg, fvh, fvi, fvj, fvk, fvl, fvm, fvn, fvo, fvp, fvq, fvr, fvs, fvt, fvu, fvv, fvw, fvx, fwz, gcc, hbm, icd, icf, icm, isq, isx, itv, jbw, jst, kea, lbt, lev, lfm, los, ltj, ltl, lul, maz, mft, mgg, mog, mot, mou, mvy, nab, nat, nip, nol, nom, noq, nor, off, omy, oso, phi, pth, ptr, pts, qms, rae, sas, sat, sca, sdt, sie, srb, ssa, ssb, ssc, ssd, sse, ssf, thh, thj, tof, tpd, tsc, ubo, ucn, vfi, wbl, wei, wut, xad, xai, xda, xik, yug, zec

3.4 PCN-6'

As described in the main text, after analysis **tbo** turns out to be the most probable topology, followed by **pto**, and **bor**; this result is in agreement with literature, where **tbo** was the assigned topology. However, PCN-6'^{21,22} has been generated at all three topologies and optimized via DFT (See Computational Details) to get some insights into the energetics and

computational PXRD pattern similarity to the **tbo**-PCN-6'. It turned out that **pto**, **bor**, and **tbo** were successfully optimized at the DFT level, providing the energy differences in agreement with experimental observation. Energetically, **tbo** is the most stable, followed by the isoenergetic **pto** just 0.5 kcal/mol, and finally **bor** 13.9 kcal/mol higher than **tbo**.

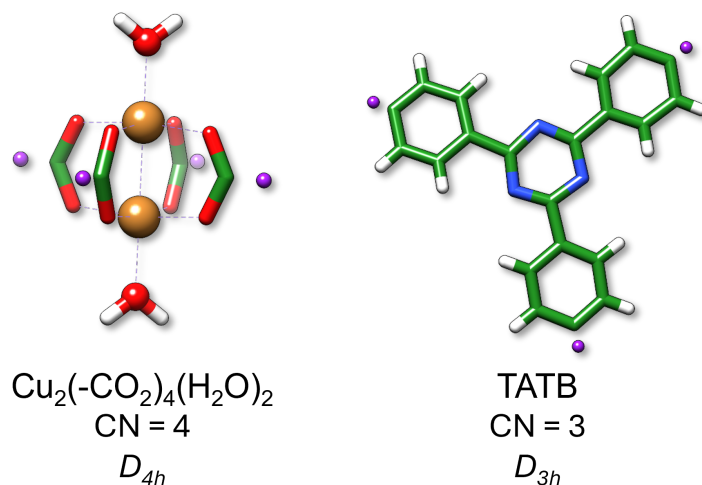


Figure S6: SBUs building blocks of MOF PCN-6'.

The full list of the 72 available topologies for connections 3 and 4 are: **afx**, **afy**, **aht**, **apc**, **apd**, **asf**, **ast**, **asv**, **att**, **atv**, **aww**, **baa**, **bab**, **bac**, **baf**, **bag**, **bah**, **baj**, **bak**, **bal**, **bam**, **ban**, **bao**, **bap**, **baq**, **bar**, **bas**, **bat**, **bau**, **bav**, **baw**, **bax**, **bay**, **baz**, **bba**, **bbb**, **bbc**, **bbd**, **bbe**, **bbf**, **bbg**, **bbh**, **bbi**, **bbj**, **bbk**, **bbm**, **bbn**, **bbo**, **bbp**, **bbq**, **bbr**, **bbs**, **bbv**, **bbw**, **bbx**, **bbz**, **bca**, **ccb**, **bcd**, **bce**, **bcf**, **bcj**, **bck**, **bcm**, **bcn**, **bco**, **bcp**, **bcq**, **bcv**, **bcw**, **bcx**, **bcy**, **bcz**, **bda**, **bel**, **bik**, **bne**, **bnl**, **bow**, **brl**, **bsv**, **byl**, **cbt**, **cda**, **cdm**, **cdn**, **cdp**, **cdz**, **cfc**, **coe**, **css**, **cua**, **cus**, **eab**, **edi**, **edp**, **eri**, **fel**, **fgl**, **frl**, **ftc**, **ftd**, **fte**, **ftf**, **ftg**, **fth**, **fti**, **ftj**, **ftk**, **ftl**, **ftm**, **ftn**, **fto**, **ftp**, **ftq**, **ftr**, **fts**, **ftt**, **ftu**, **ftv**, **ftx**, **fty**, **ftz**, **fua**, **fub**, **fud**, **fue**, **fuf**, **fug**, **fuh**, **fuj**, **ful**, **fum**, **fun**, **fuo**, **fup**, **fur**, **fus**, **fut**, **fuu**, **fuv**, **fuw**, **fuy**, **fuz**, **fva**, **fvb**, **fvc**, **fvd**, **fve**, **fvf**, **fvh**, **fvi**, **fvj**, **fvk**, **fvn**, **fvo**, **fvp**, **fvq**, **fvr**, **fvs**, **fvt**, **fvu**, **fvv**, **fvw**, **fvx**, **fwz**, **gcc**, **hbm**, **icd**, **icf**, **icm**, **isq**, **isx**, **itv**, **jbw**, **jst**, **kea**, **lbt**, **lev**, **lfm**, **los**, **ltj**, **ltl**, **lul**, **maz**, **mft**, **mgg**, **mog**, **mot**, **mou**, **mvy**, **nab**, **nat**, **nip**, **nol**, **nom**, **noq**, **nor**, **off**, **omy**, **oso**, **phi**, **pth**,

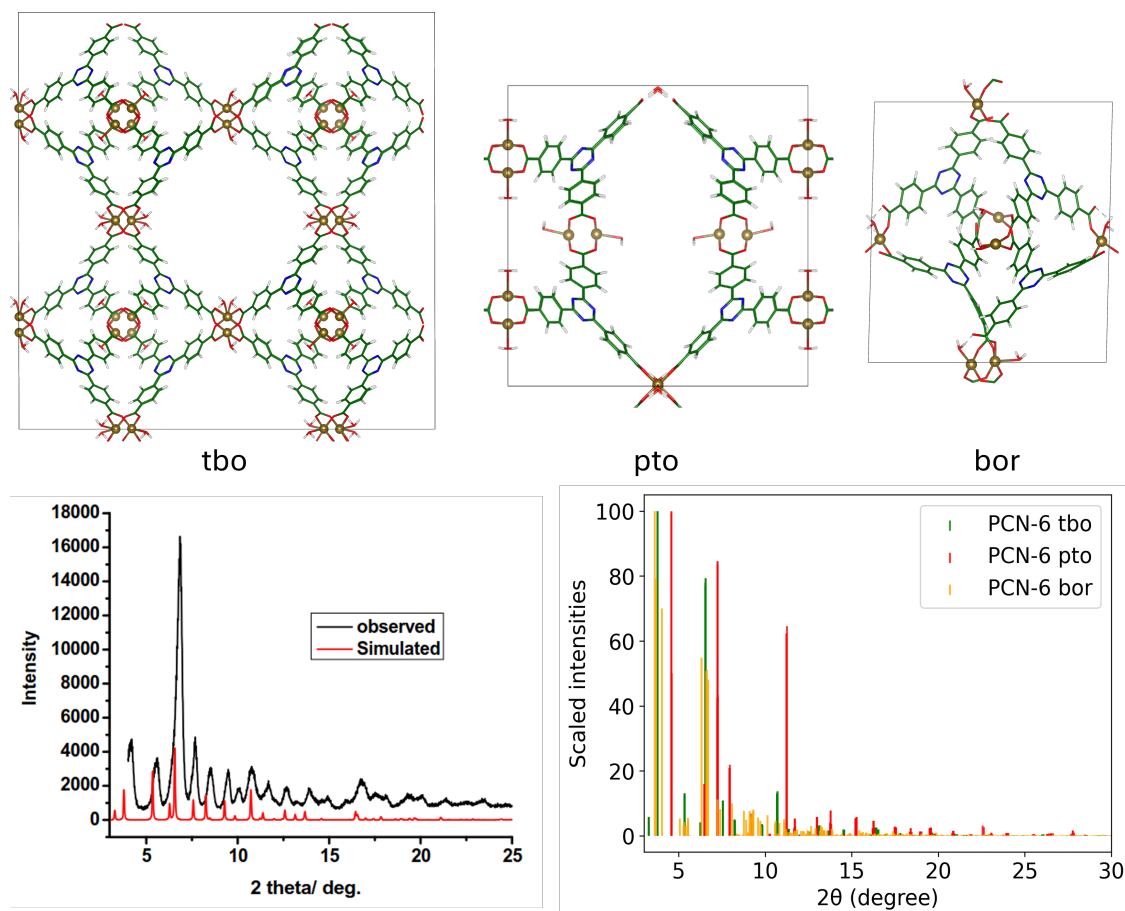


Figure S7: **tbo**-PCN-6', **pto**-PCN-6', and **bor**-PCN-6' optimized structures at DFT level (top), with respective computational PXRD patterns (bottom right), and experimental PXRD pattern from reference [21] (bottom left).

ptr, pts, qms, rae, sas, sat, sca, sdt, sie, srb, ssa, ssb, ssc, ssd, sse, ssf, thh, thj, tof, tpd, tsc, ubo, ucn, vfi, wbl, wei, wut, xad, xai, xda, xik, yug, zec

3.5 LZU-306

As a COF example, the non interpenetrated material LZU-306 has been chosen.²³ It is formed by condensation of a tetraphenylethylene based (TPE-NH₂) quadrilateral linker, and an adamantane based (ADA-CHO) *quasi*-tetrahedral node, both with connections number 4 (CN = 4) (SBUs shown in Figure S8). The coupling of two building blocks with 4 connections each provides the same available topologies as the previously described NU-50. The same procedure described in the main text was followed. The ADA-CHO node has D_{2d} symmetry,

and the TPE-NH₂ linker has D_2 symmetry. Including also the corresponding higher (node D_{4h} , linker D_{2h}) and lower (node D_2 , linker C_2) symmetry groups, the selected topologies are: **pts**, **css**, **pth**, **icd**, **ssa**, **ssb**, **ssc**. Ranking by frequency of occurrence provides the following order: **pts** (D_{2d} and D_{2h} , 30461, exp: 262), **ssb** (D_2 and D_2 , 1765, exp: 9), **pth** (D_2 and D_2 , 297, exp: 3), and **ssa** (D_2 and D_2 , 108, exp: 13); with **pts** in first position in agreement with experimental findings in both ARC-derived and experimental dataset.²³ The only difference between the dataset is the ranking after the first position where **ssa** and **ssb** are ranking in second and third position respectively, rather than fourth and second.

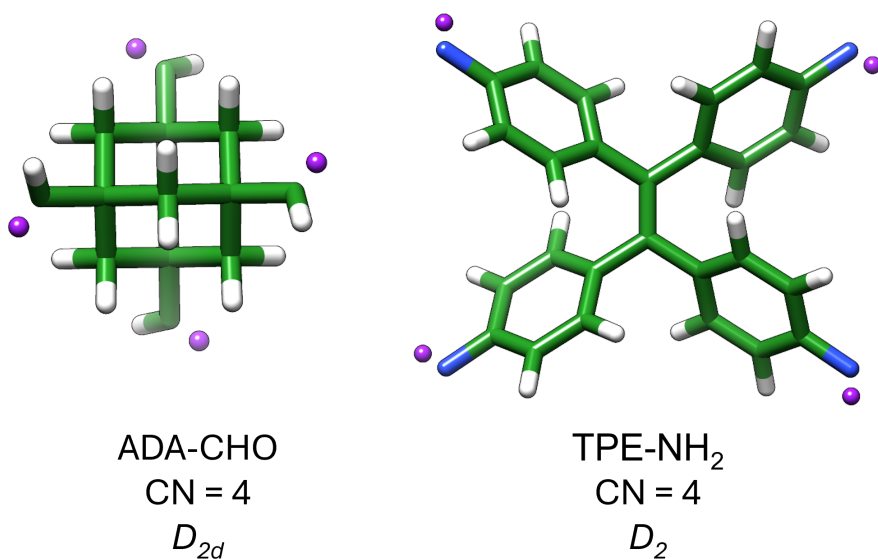


Figure S8: SBUs building blocks of COF LZU-306.

3.6 LZU-111

In this section the complete computational PXRD pattern are shown from manually generated LZU-111 **lon-b** 3-, 2-, and non- interpenetrated structures, and **pts** structure in Figure S9, together with the experimentally published PXRD pattern.²⁴

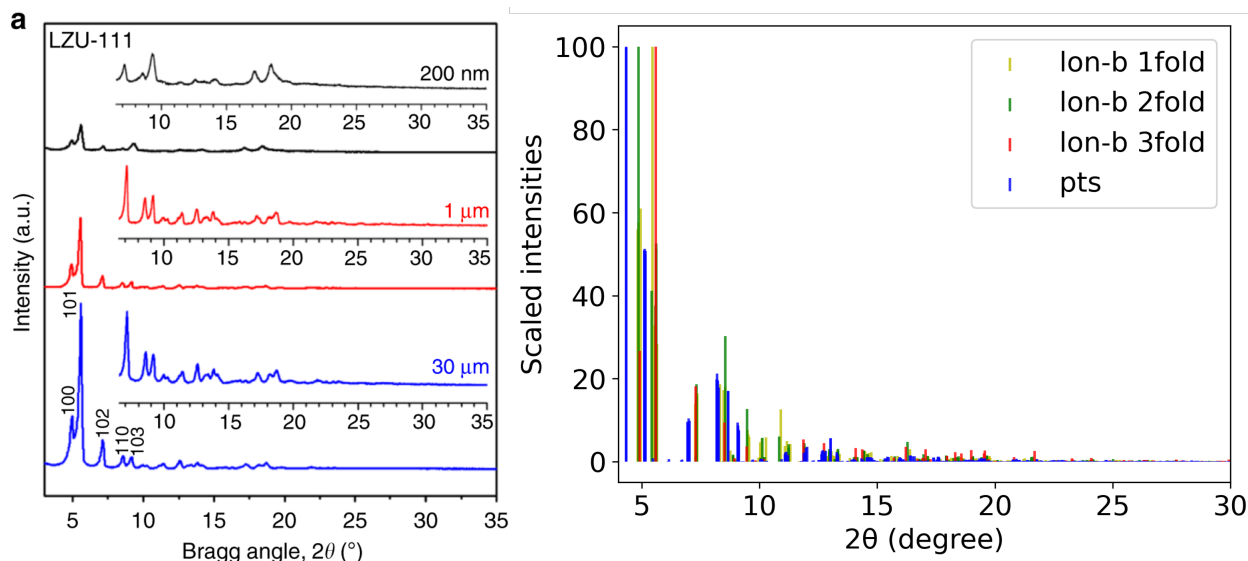


Figure S9: PXRD pattern from experiments (l. h. s.) of **lon-b** 3-fold interpenetrated LZU-111 from reference [24]; and computationally calculated (r. h. s.) PXRD pattern of **pts**, **lon-b** 3-, 2-, and non- interpenetrated LZU-111 structures.

Energetically **lon-b-3c**-LZU-111 is the most stable followed by **lon-b-2c**-LZU-111 at 12.7 kcal/mol, **lon-b-1c**-LZU-111 at 24.4 kcal/mol, and **pts**-LZU-111 at 61.3 kcal/mol.

4 CSD Refcodes

Although this work is fully computational with reticular frameworks structures made in silico from scratch, the comparison with PXRD patterns uses plots from experiments. Therefore the related refcode of such structures are listed here:

- MOF-801: BOHKAM
- MOF-802: BOHXED

- MOF-812: BOHWOM
- MOF-841: BOHWIG
- MOF-808: BOHWUS
- NU-50: VEDJOH
- PCN-6': NIBHOW
- UIO-66: RUBTAK
- LZU-306: no refcode, coordinates available in the supp. material of ref [23]
- LZU-111: RIHZAM

References

- (1) Kresse, G.; Furthmüller, J.; Hafner, J. Theory of the crystal structures of selenium and tellurium: the effect of generalized-gradient corrections to the local-density approximation. *Phys. Rev. B.* (**1994**), 13181.
- (2) Kresse, G.; Furthmüller, J. Efficiency of ab-initio total energy calculations for metals and semiconductors using a plane-wave basis set. *Comput. Mater. Sci.* (**1996**), 15–50.
- (3) Kresse, G.; Furthmüller, J. Efficiency of ab-initio total energy calculations for metals and semiconductors using a plane-wave basis set. *Comput. Mater. Sci.* (**1996**), 15–50.
- (4) Perdew, J. P.; Burke, K.; Ernzerhof, M. Generalized gradient approximation made simple. *Phys. Rev. Lett.* (**1996**), 3865.
- (5) Grimme, S.; Ehrlich, S.; Goerigk, L. Effect of the damping function in dispersion corrected density functional theory. *J. Comput. Chem.* (**2011**), 1456–1465.

- (6) Furness, J. W.; Kaplan, A. D.; Ning, J.; Perdew, J. P.; Sun, J. Accurate and numerically efficient r2SCAN meta-generalized gradient approximation. *J. Phys. Chem. Lett.* (**2020**), 8208–8215.
- (7) Ning, J.; Kothakonda, M.; Furness, J. W.; Kaplan, A. D.; Ehlert, S.; Brandenburg, J. G.; Perdew, J. P.; Sun, J. Workhorse minimally empirical dispersion-corrected density functional with tests for weakly bound systems: r²SCAN + rVV10. *Phys. Rev. B.* (7 **2022**), 075422.
- (8) Kresse, G.; Joubert, D. From ultrasoft pseudopotentials to the projector augmented-wave method. *Phys. rev. B.* (**1999**), 1758.
- (9) Frisch, M. J.; Trucks, G. W.; Schlegel, H. B.; Scuseria, G. E.; Robb, M. A.; Cheeseman, J. R.; Scalmani, G.; Barone, V.; Petersson, G. A.; Nakatsuji, H.; Li, X.; Caricato, M.; Marenich, A. V.; Bloino, J.; Janesko, B. G.; Gomperts, R.; Mennucci, B.; Hratchian, H. P.; Ortiz, J. V.; Izmaylov, A. F.; Sonnenberg, J. L.; Williams-Young, D.; Ding, F.; Lipparini, F.; Egidi, F.; Goings, J.; Peng, B.; Petrone, A.; Henderson, T.; Ranasinghe, D.; Zakrzewski, V. G.; Gao, J.; Rega, N.; Zheng, G.; Liang, W.; Hada, M.; Ehara, M.; Toyota, K.; Fukuda, R.; Hasegawa, J.; Ishida, M.; Nakajima, T.; Honda, Y.; Kitao, O.; Nakai, H.; Vreven, T.; Throssell, K.; Montgomery Jr., J. A.; Peralta, J. E.; Ogliaro, F.; Bearpark, M. J.; Heyd, J. J.; Brothers, E. N.; Kudin, K. N.; Staroverov, V. N.; Keith, T. A.; Kobayashi, R.; Normand, J.; Raghavachari, K.; Rendell, A. P.; Burant, J. C.; Iyengar, S. S.; Tomasi, J.; Cossi, M.; Millam, J. M.; Klene, M.; Adamo, C.; Cammi, R.; Ochterski, J. W.; Martin, R. L.; Morokuma, K.; Farkas, O.; Foresman, J. B.; Fox, D. J. Gaussian 16 Revision B.01, 2016.
- (10) Tao, J.; Perdew, J. P.; Staroverov, V. N.; Scuseria, G. E. Climbing the density functional ladder: Nonempirical meta-generalized gradient approximation designed for molecules and solids. *Phys. Rev. Lett.* (**2003**), 146401.

- (11) Staroverov, V. N.; Scuseria, G. E.; Tao, J.; Perdew, J. P. Comparative assessment of a new nonempirical density functional: Molecules and hydrogen-bonded complexes. *J. Chem. Phys.* (**2003**), 12129–12137.
- (12) Weigend, F.; Ahlrichs, R. Balanced basis sets of split valence, triple zeta valence and quadruple zeta valence quality for H to Rn: Design and assessment of accuracy. *Phys. Chem. Chem. Phys.* (18 **2005**), 3297–3305.
- (13) Burner, J.; Luo, J.; White, A.; Mirmiran, A.; Kwon, O.; Boyd, P. G.; Maley, S.; Gibaldi, M.; Simrod, S.; Ogden, V.; Woo, T. K. ARC–MOF: A Diverse Database of Metal–Organic Frameworks with DFT-Derived Partial Atomic Charges and Descriptors for Mach. Learn. *Chem. Mater.* (**2023**), 900–916.
- (14) Bonneau, C.; O’Keeffe, M.; Proserpio, D. M.; Blatov, V. A.; Batten, S. R.; Bourne, S. A.; Lah, M. S.; Eon, J.-G.; Hyde, S. T.; Wiggin, S. B.; Öhrström, L. Deconstruction of Crystalline Networks into Underlying Nets: Relevance for Terminology Guidelines and Crystallographic Databases. *Cryst. Growth Des.* (**2018**), 3411–3418.
- (15) Chung, Y. G.; Haldoupis, E.; Bucior, B. J.; Haranczyk, M.; Lee, S.; Zhang, H.; Vogiatzis, K. D.; Milisavljevic, M.; Ling, S.; Camp, J. S.; Slater, B.; Siepmann, J. I.; Sholl, D. S.; Snurr, R. Q. Advances, Updates, and Analytics for the Computation-Ready, Experimental Metal–Organic Framework Database: CoRE MOF 2019. *J. Chem. Eng. Data* (**2019**), 5985–5998.
- (16) Moghadam, P. Z.; Li, A.; Wiggin, S. B.; Tao, A.; Maloney, A. G. P.; Wood, P. A.; Ward, S. C.; Fairen-Jimenez, D. Development of a Cambridge Structural Database Subset: A Collection of Metal–Organic Frameworks for Past, Present, and Future. *Chemistry of Materials* (**2017**), 2618–2625.
- (17) Li, A.; Perez, R. B.; Wiggin, S.; Ward, S. C.; Wood, P. A.; Fairen-Jimenez, D. The launch of a freely accessible MOF CIF collection from the CSD. *Matter* (**2021**), 1105–1106.

- (18) Furukawa, H.; Gándara, F.; Zhang, Y.-B.; Jiang, J.; Queen, W. L.; Hudson, M. R.; Yaghi, O. M. Water Adsorption in Porous Metal–Organic Frameworks and Related Mater. *J. Am. Chem. Soc.* (**2014**), 4369–4381.
- (19) Cavka, J. H.; Jakobsen, S.; Olsbye, U.; Guillou, N.; Lamberti, C.; Bordiga, S.; Lillerud, K. P. A new zirconium inorganic building brick forming metal organic frameworks with exceptional stability. *J. Ame. Chem. Soc.* (**2008**), 13850–13851.
- (20) Chen, Y.; Zhang, X.; Chen, H.; Drout, R. J.; Chen, Z.; Mian, M. R.; Maldonado, R. R.; Ma, K.; Wang, X.; Xia, Q.; Li, Z.; Islamoglu, T.; Snurr, R. Q.; Farha, O. K. Tuning the Atrazine Binding Sites in an Indium-Based Flexible Metal–Organic Framework. *ACS Appl. Mater. Interfaces.* (**2020**), 44762–44768.
- (21) Sun, D.; Ma, S.; Ke, Y.; Collins, D. J.; Zhou, H.-C. An Interweaving MOF with High Hydrogen Uptake. *J. Am. Chem. Soc.* (**2006**), 3896–3897.
- (22) Ma, S.; Sun, D.; Ambrogio, M.; Fillinger, J. A.; Parkin, S.; Zhou, H.-C. Framework-Catenation Isomerism in Metal–Organic Frameworks and Its Impact on Hydrogen Uptake. *J. Am. Chem. Soc.* (**2007**), 1858–1859.
- (23) Liang, L.; Qiu, Y.; Wang, W. D.; Han, J.; Luo, Y.; Yu, W.; Yin, G.-L.; Wang, Z.-P.; Zhang, L.; Ni, J.; Niu, J.; Sun, J.; Ma, T.; Wang, W. Non-Interpenetrated Single-Crystal Covalent Organic Frameworks. *Angew. Chem. Int. Ed.* (**2020**), 17991–17995.
- (24) Ma, T.; Wei, L.; Liang, L.; Yin, S.; Xu, L.; Niu, J.; Xue, H.; Wang, X.; Sun, J.; Zhang, Y.-B., et al. Diverse crystal size effects in covalent organic frameworks. *Nat. Commun.* (**2020**), 6128.